Supplementary Information (SI) for Journal of Materials Chemistry A.
This journal is © The Royal Society of Chemistry 2026

Supplementary Material

Engineering High-Valent Ni^{3+}–O Active Sites through Pd Incorporation in NiCo-MOF/Ni-Foam for Enhanced 5-Hydroxymethylfurfural Electrooxidation

Zijian Liu[a], Chunli Xie[a], Yuanhong Zhong[a, b*], Yingxia Zhao, Sisi Xiang[a], Ming Sun[a, b], Lin Yu[a,b]

[a]Key Laboratory of Clean Chemistry Technology of Guangdong Regular Higher Education Institutions, Guangdong Engineering Technology Research Center of Modern Fine Chemical Engineering, School of Chemical Engineering and Light Industry, Guangdong University of Technology, Guangzhou 510006, P. R. China

[b]Jieyang Branch of Chemistry and Chemical Engineering Guangdong Laboratory (Rongjiang Laboratory), Jieyang 515200, P. R. China

E-mail: zhongyuanhong@gdut.edu.cn

Contents

Text S1. Materials and chemicals

$Ni(NO_3)_2 \cdot 6H_2O$ (99%), $Co(NO_3)_2 \cdot 6H_2O$ (99%), 2-methylimidazole (2-MI), methanol (CH_3OH, 99.99%), $PdCl_2$, and KOH (95%) were purchased from Sigma-Aldrich (USA). 5-Hydroxymethylfurfural (HMF, 99%), furan-2,5-dicarbaldehyde (DFF, 98%), 5-hydroxymethyl-2-furancarboxylic acid (HMFCA, 98%), 5-formyl-2-furancarboxylic acid (FFCA, >98%), and 2,5-furandicarboxylic acid (FDCA, 98%) were obtained from Aladdin Reagent Co., Ltd. (China). All reagents were used as received without further purification. The nickel foam (NF, 1 × 3 cm^2) was ultrasonicated in 3 mmol L^{-1} HCl solution, ethanol (C_2H_6O), and deionized (DI) water for 20 min sequentially. Then dried in the vacuum oven at 60 ℃ for 12 hours.

Text S2. Characterization of the catalyst

The morphology of the catalyst samples was characterized by scanning electron microscopy (SEM, FEI Nova Nano SEM 450) and transmission electron microscopy (TEM, FEI Chennai F20). The crystalline phase composition was analyzed by X-ray diffraction (XRD, Panalytical Aeris) using Cu Kα radiation, with a scan rate of 5° min^{-1} over a 5°–60° range. X-ray photoelectron spectroscopy (XPS; Escalab 250Xi, Thermo Fisher) was employed to examine the surface chemical states, using an Al Kα (650 μm) source at 15 kV and 15 mA, with the C 1s peak at 284.8 eV (C–C bond) as the reference for calibration. Elemental composition was determined by inductively coupled plasma optical emission spectroscopy (ICP-OES, Agilent 5110).

Text S3. Electrochemical measurements

Linear-sweep voltammograms (LSV) were acquired at 5 mV s^{-1} without iR compensation. The electrochemically active surface area (ECSA) was determined from

the double-layer capacitance (C_{dl}), measured by cyclic voltammetry (CV) in the non-faradaic region at scan rates of 20, 40, 60, 80, 100, and 120 mV s^{-1} in 1.0 mol L^{-1} KOH electrolyte with 30 mmol L^{-1} HMF. C_{dl} was extracted from the linear slope of capacitive current versus scan rate, and ECSA was calculated using Eq. (1).

$$ECSA = C_{dl}/C_s \quad (1)$$

where Cs = 40 μF cm^{-2} denotes the specific double-layer capacitance of an ideal planar electrode. In-situ electrochemical impedance spectroscopy (EIS) was performed from 10^5 to 0.1 Hz (5 mV alternating Current perturbation) as the applied potential was stepped from 1.10 to 1.55 V.

Text S4. Products analysis

HMF electro-oxidation was carried out by chronoamperometry at 1.4 V in an H-type cell: the anodic compartment held 10 mL of 1.0 mol L^{-1} KOH containing 10.0 mmol L^{-1} HMF, while the cathodic compartment contained 10 mL of 1.0 M KOH. Progress was monitored by withdrawing 20 μL aliquots from the anolyte and diluting each to 1.5 mL with K_2CO_3 solution for subsequent analysis. The composition of the reaction mixture was analyzed using a Shimadzu high-performance liquid chromatography (HPLC) system equipped with an SPD-M40 UV detector, a CTO-40S column oven, and a C18 column (4.6 mm × 250 mm, 5 μm). The mobile phase consisted of a mixed solution of 20% acetonitrile and 80% 0.1 *wt*% aqueous acetic acid. The column temperature was maintained at 50 °C, with a flow rate of 0.5 mL min^{-1}. Quantitative analysis employed an external-standard calibration: HMFCA and FDCA were monitored at 254 nm, whereas HMF and FFCA were quantified at 285 nm.

The theoretical total charge for the electro-oxidation of HMF was calculated as:

$$6 \times 10\ mL \times 10\ mmol\ L^{-1} \times 96485\ C\ mol^{-1} = 57.9\ (C) \quad (1)$$

The HMF conversion rate, FDCA yield, and Faradaic efficiency (*FE*) of products were calculated by using the following formulas:

$$\text{Conversion of HMF (\%)} = \frac{n\ (\text{HMF consumed})}{n\ (\text{initial HMF})} \times 100\% \quad (2)$$

$$\text{Yield of FDCA (\%)} = \frac{n\ (\text{FDCA formed})}{n\ (\text{initial HMF})} \times 100\% \quad (3)$$

$$\text{Selectivity of product (\%)} = \frac{n\ (\text{product})}{n\ (\text{consumed HMF})} \times 100\% \quad (4)$$

$$FE\ (\%) = \frac{N \times \text{F} \times n\ (\text{FDCA formed})}{\text{total charge passed}} \times 100\% \quad (5)$$

Where n is the molar amount of HMF or its products, N is the number of transferred electrons, which is 6, and F is the Faraday constant (96485 C mol^{-1}).

Text S5. Density functional theory (DFT) calculations

Spin-polarized density-functional theory (DFT) calculations were carried out with the Vienna Ab initio Simulation Package (VASP) using the projector-augmented wave (PAW) method. The electron-ion interactions were characterized using typical PAW potentials. The smooth component of the wave functions with a cutoff kinetic energy of 400 eV was expanded using a plane-wave basis set. The Perdew-Burke-Ernzerhof (PBE) functional, a form of the General Gradient Approximation (GGA), has been used throughout the electron-electron exchange and correlation interactions. Surface chemistry was investigated using periodic slab models separated by a 15 Å vacuum; the bottom atomic layers were fixed at bulk positions while the remaining atoms were fully relaxed. Brillouin-zone integrations employed Monkhorst–Pack k-point meshes with a 0.04 $Å^{-1}$ spacing..Self-consistency was achieved when the total energy converged within 10^{-5} eV, and structural optimizations were deemed complete when all

residual forces fell below 0.03 eV $Å^{-1}$.

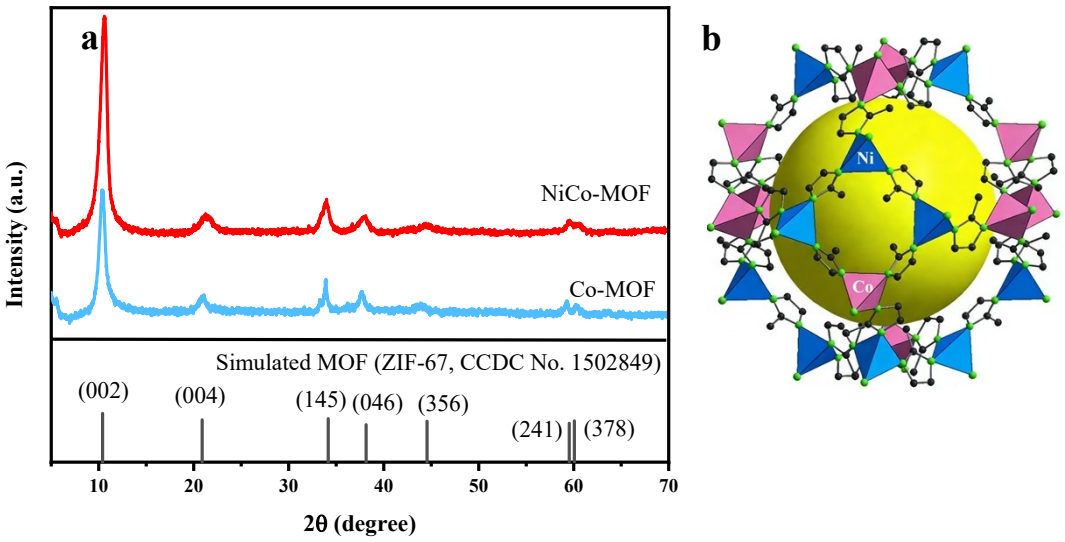

Fig. S1 (a) XRD patterns of NiCo-MOF powder sample, and (b) its structural schematic.

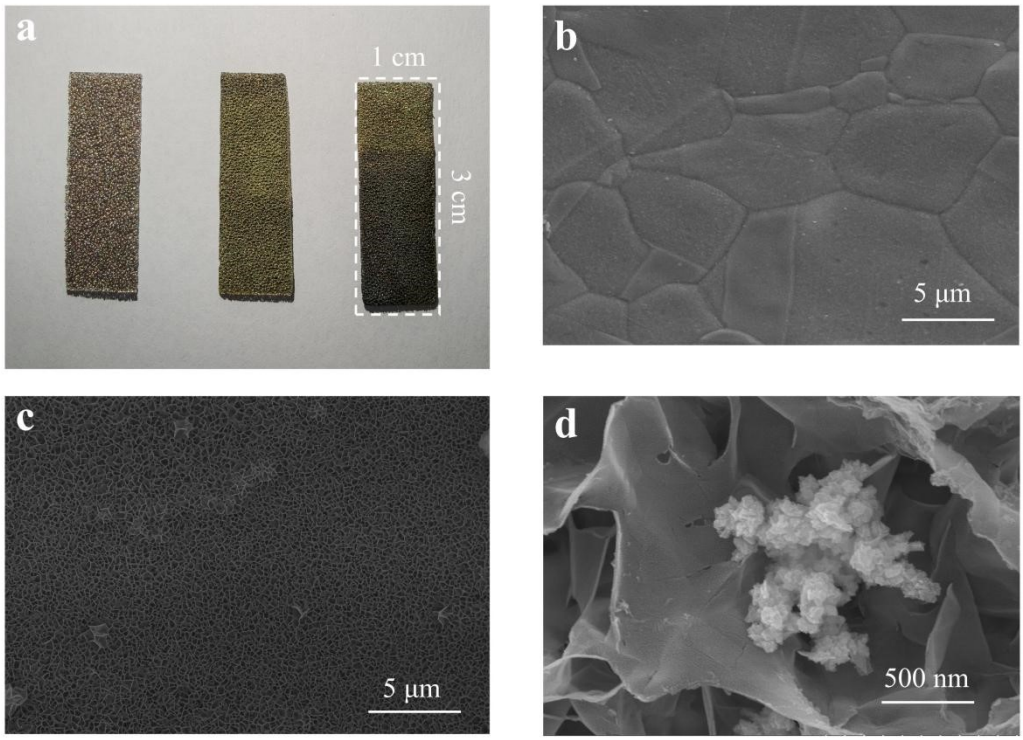

Fig. S2 (a) Optical photos and (b-d) SEM images of NF, NiCo-MOF/NF, and Pd/NiCo-MOF/NF.

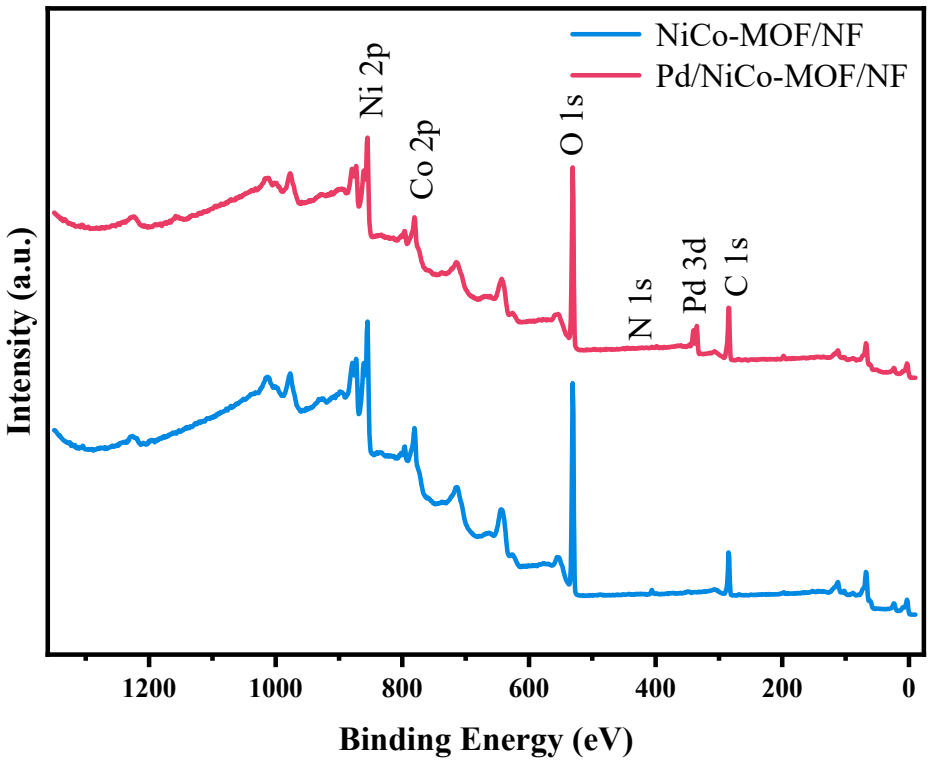

Fig. S3 Survey XPS spectra of Pd/NiCo-MOF/NF and NiCo-MOF/NF electrode.

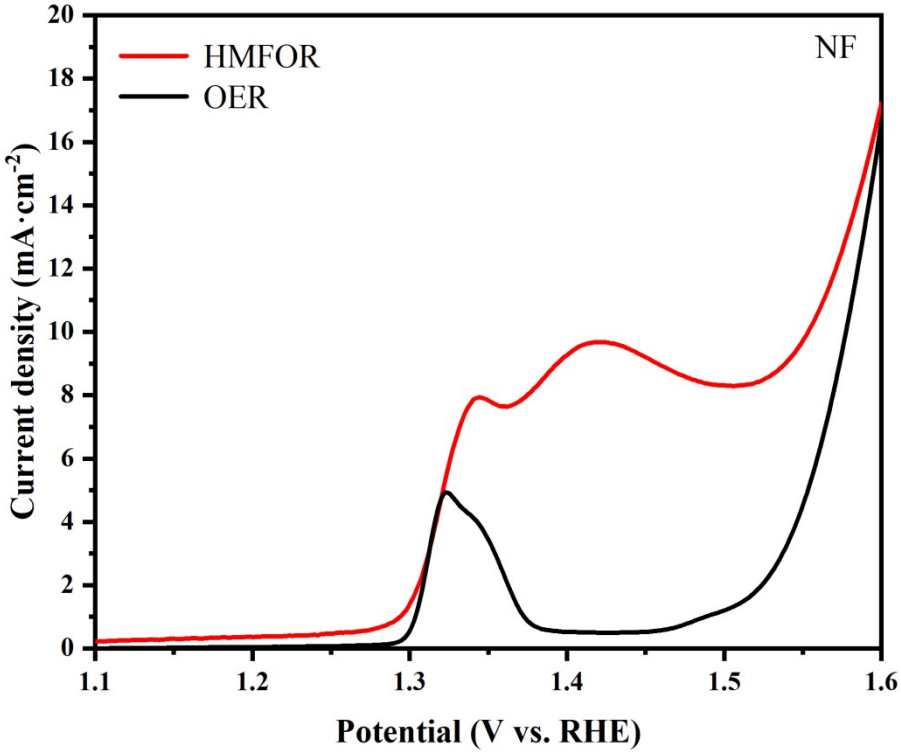

Fig. S4 LSV curves of blank NF with and without HMF.

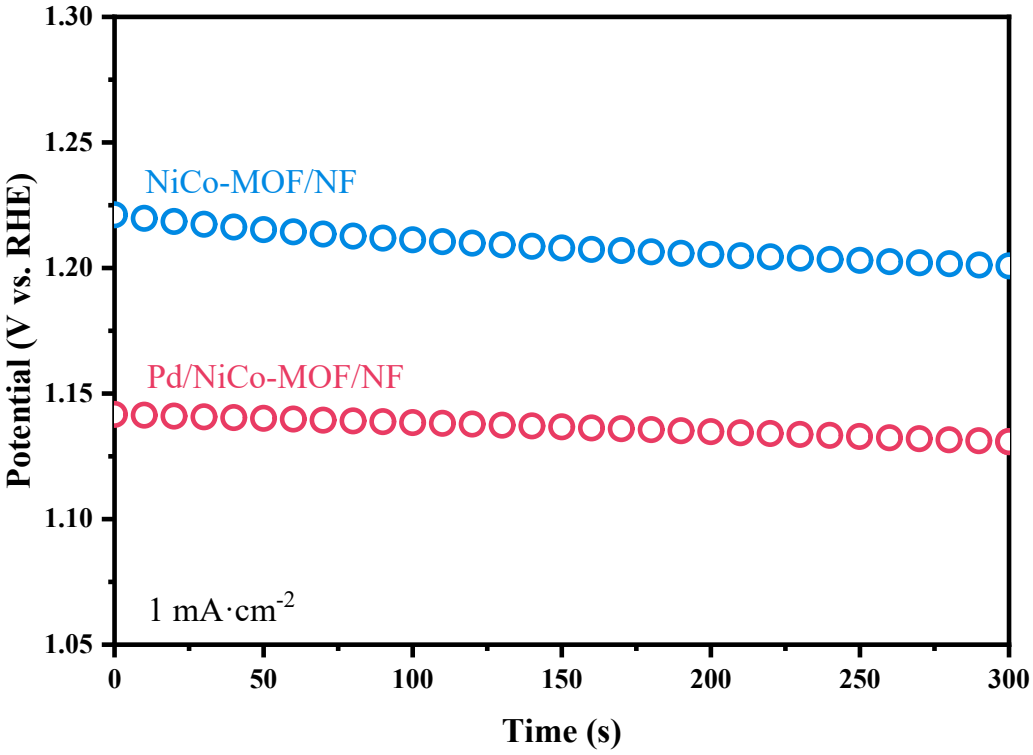

Fig. S5 Onset Potential Determination via Chronopotentiometry at 1.0 mA cm^{-2}.

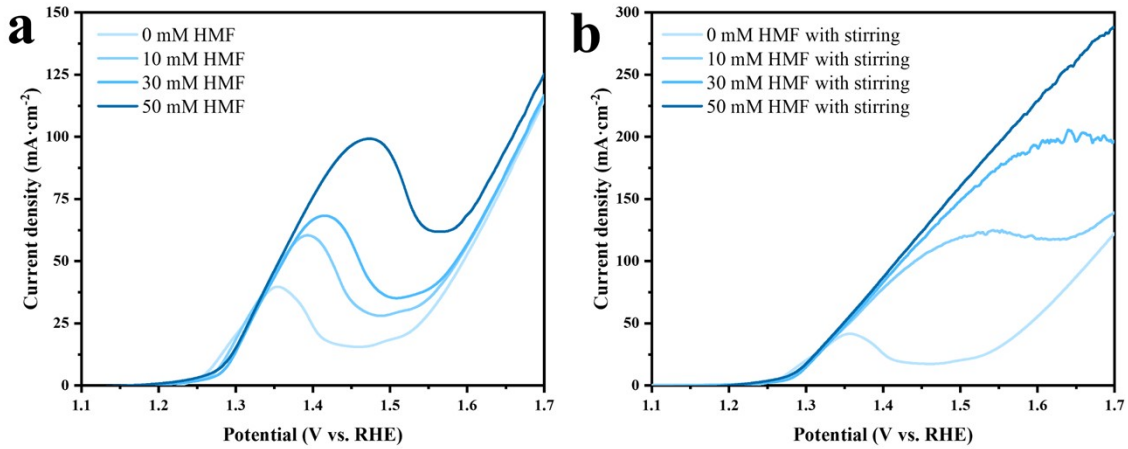

Fig. S6 LSV curves of Pd/NiCo-MOF/NF at different HMF concentrations without (a) and with (b) stirring.

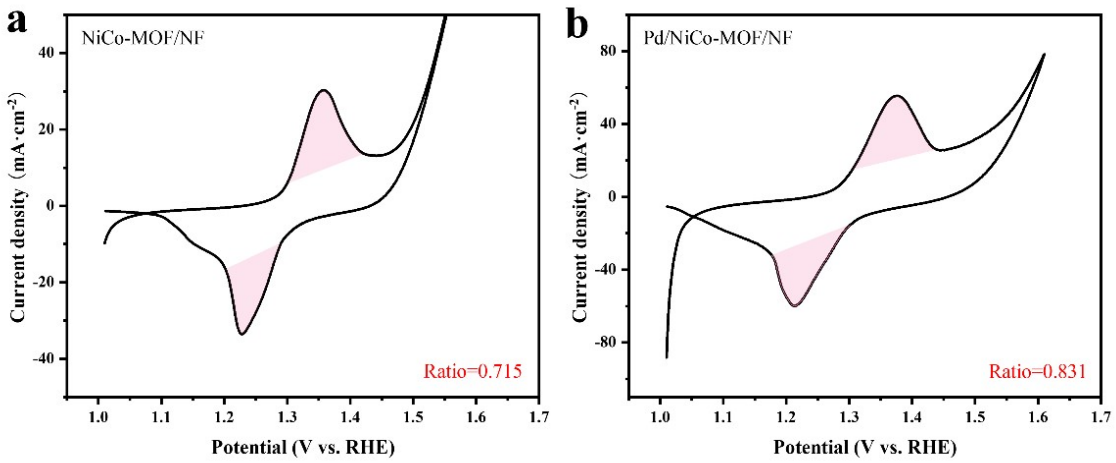

Fig. S7 CV sweeps of (a) NiCo-MOF/NF and (b) Pd/NiCo-MOF/NF at the scan rate of 5 mV s^{-1}.

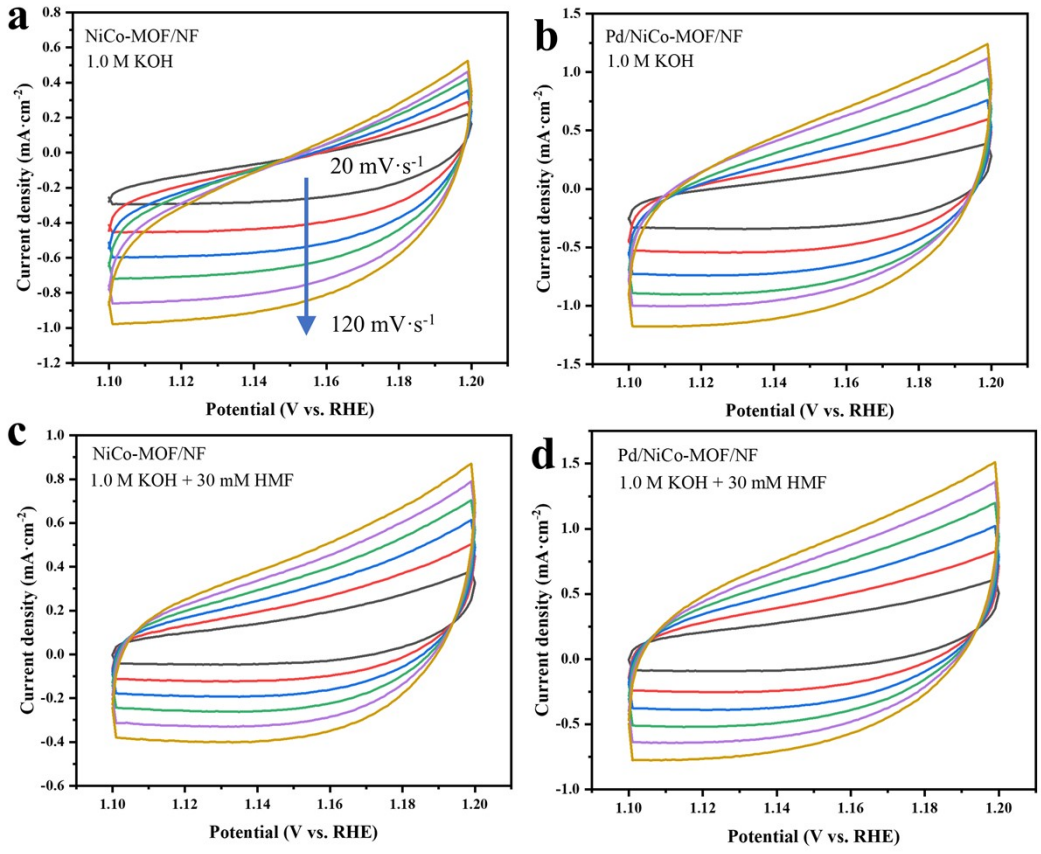

Fig. S8 CV cycles at different scanning rates at (a-b) 1.0 mol L^{-1} KOH. (c-d) 1.0 mol L^{-1} KOH with 30 mmol L^{-1} HMF.

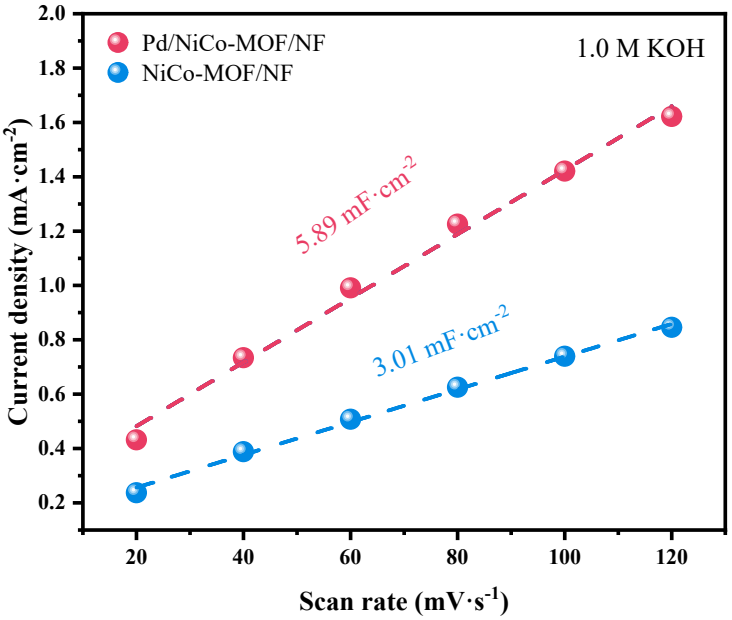

Fig. S9 C_{dl} of NiCo-MOF/NF and Pd/NiCo-MOF/NF in 1.0 mol L^{-1} KOH without adding HMF.

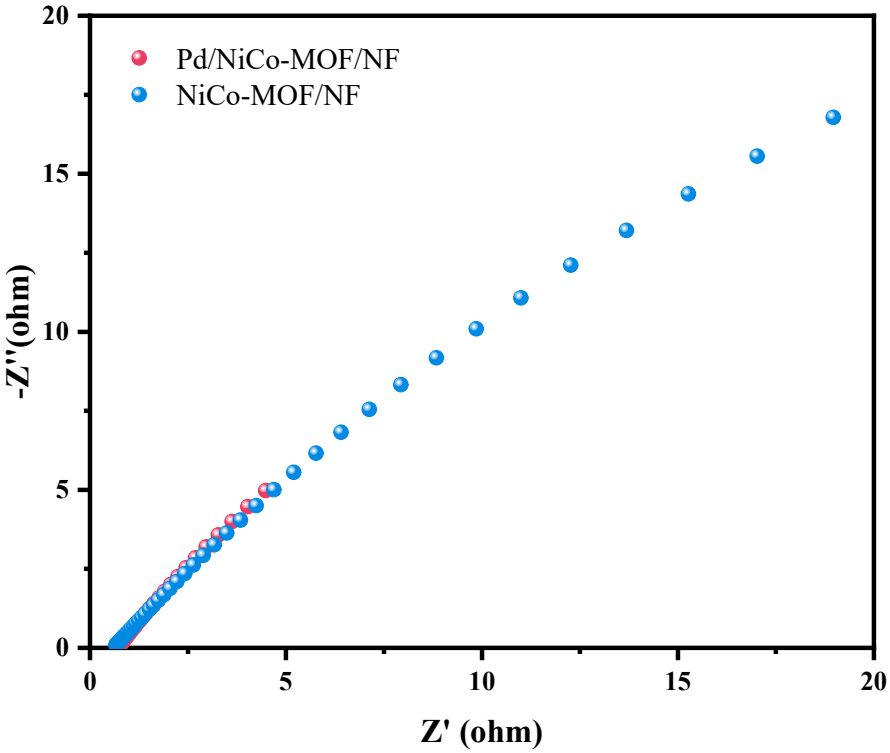

Fig. S10 EIS Nyquist plots of NiCo-MOF/NF and Pd/NiCo-MOF/NF in 1.0 mol L^{-1} KOH without HMF.

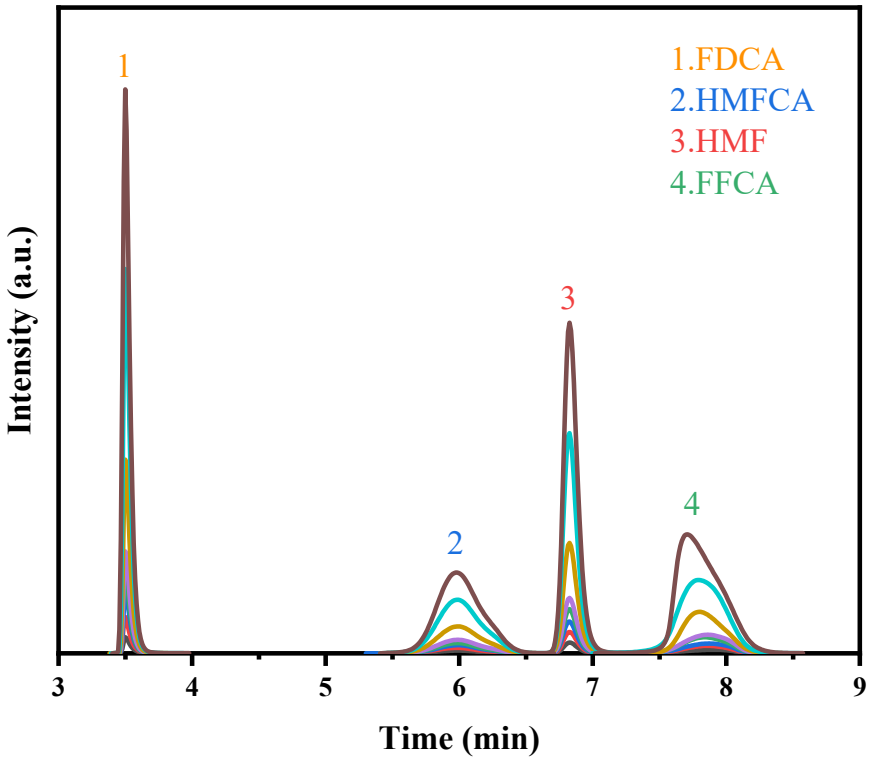

Fig. S11 HPLC chromatograms: Retention-time profiles of HMF, FDCA, HMFCA, and FFCA.

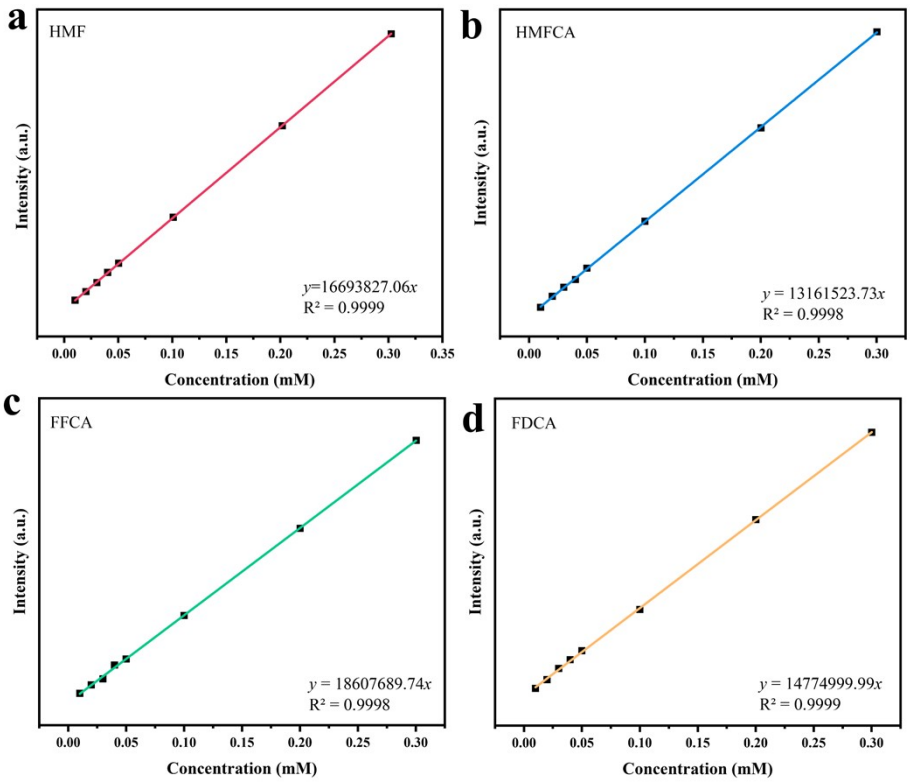

Fig. S12 HPLC calibration curves for (a) substrate HMF, (b) HMFCA, (c) FFCA, (d) FDCA, each determined over a concentration gradient.

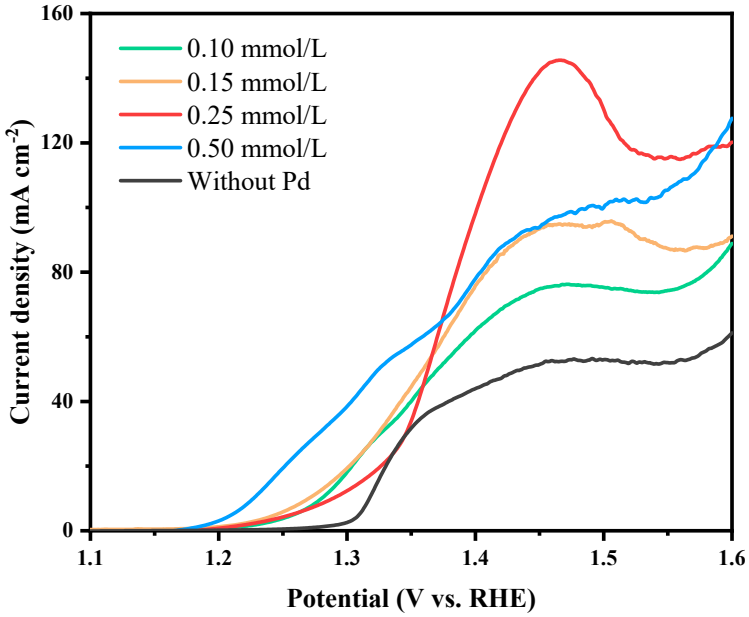

Fig. S13 LSV curves of Pd/NiCo-MOF/NF electrodes prepared using different Pd precursor concentrations (0.10, 0.15, 0.25, and 0.50 mmol L^{-1}) measured in 1.0 mol L^{-1} KOH containing 10 mmol L^{-1} HMF.

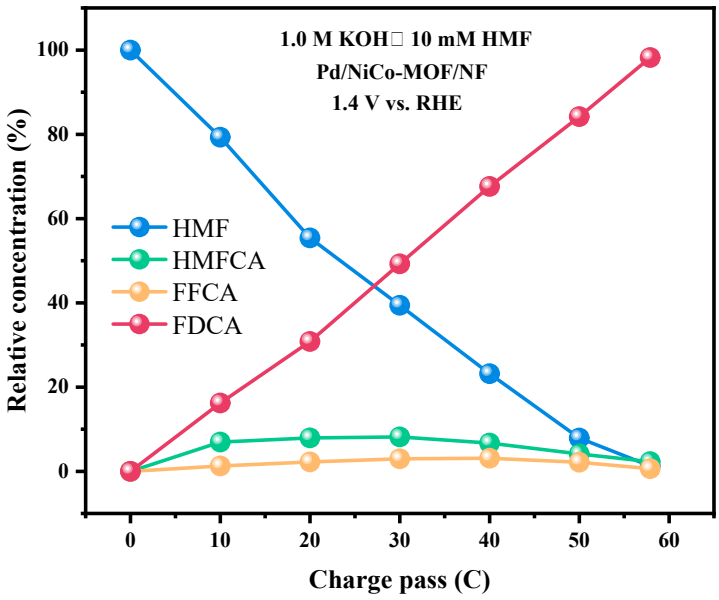

Fig. S14 Temporal concentration profiles of HMF and its oxidation products during electro-oxidation on Pd/NiCo-MOF/NF at 1.40 V *vs.* RHE.

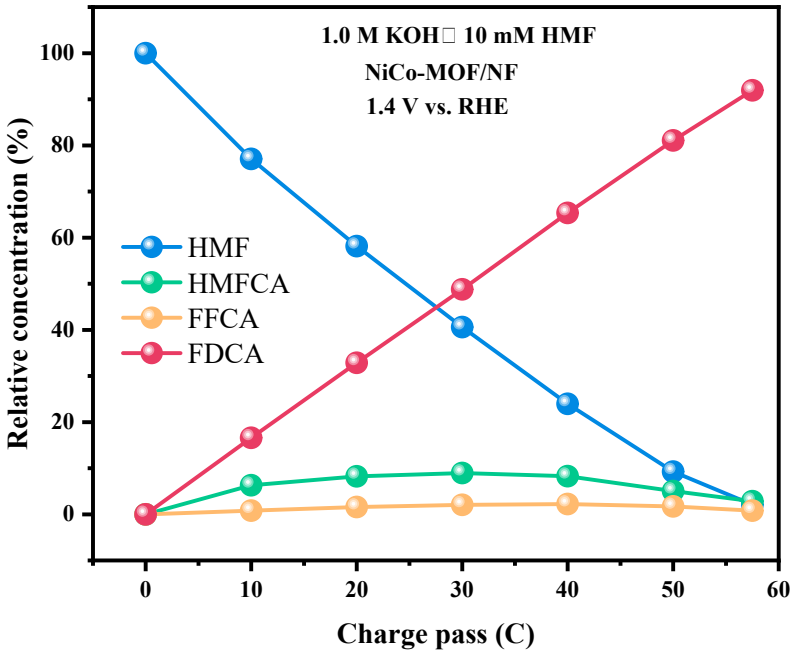

Fig. S15 Temporal concentration profiles of HMF and its oxidation products during electro-oxidation on NiCo-MOF/NF at 1.40 V *vs.* RHE.

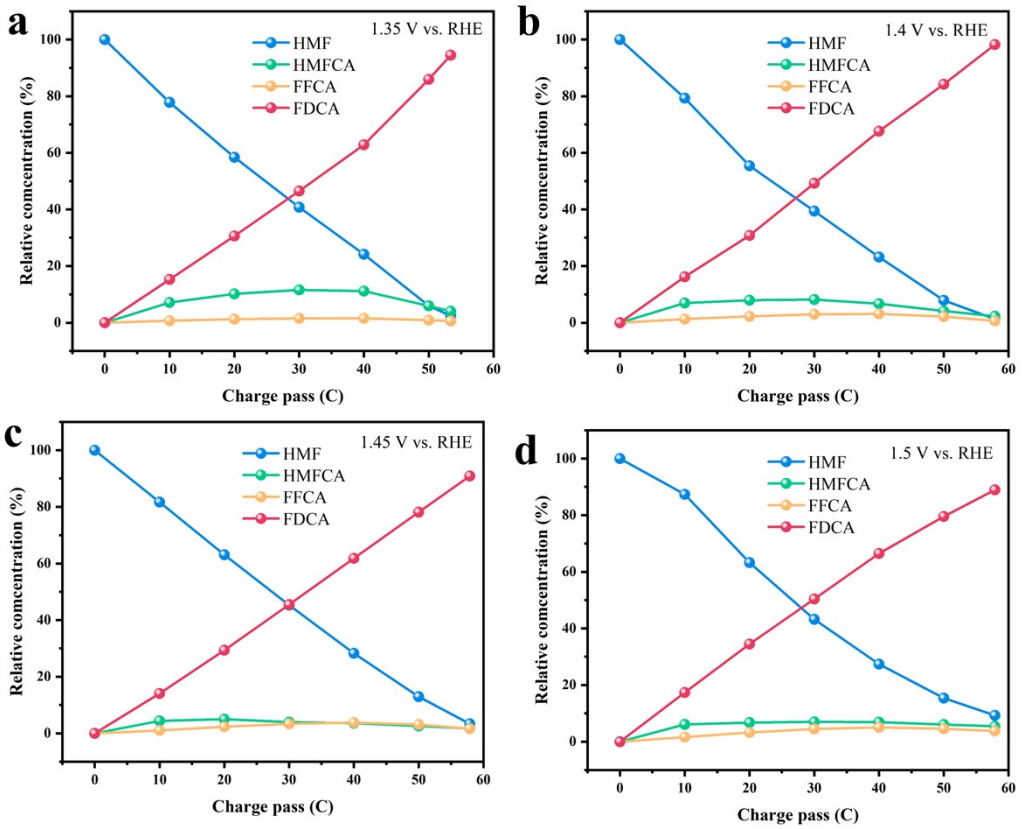

Fig. S16 The concentration changes of HMF and its oxidation products during HMF electro-oxidation when using Pd/NiCo-MOF/NF catalyst at (a) 1.35 V *vs.* RHE, (b) 1.40 V *vs.* RHE, (c) 1.45 V *vs.* RHE, (d) 1.50 V *vs.* RHE.

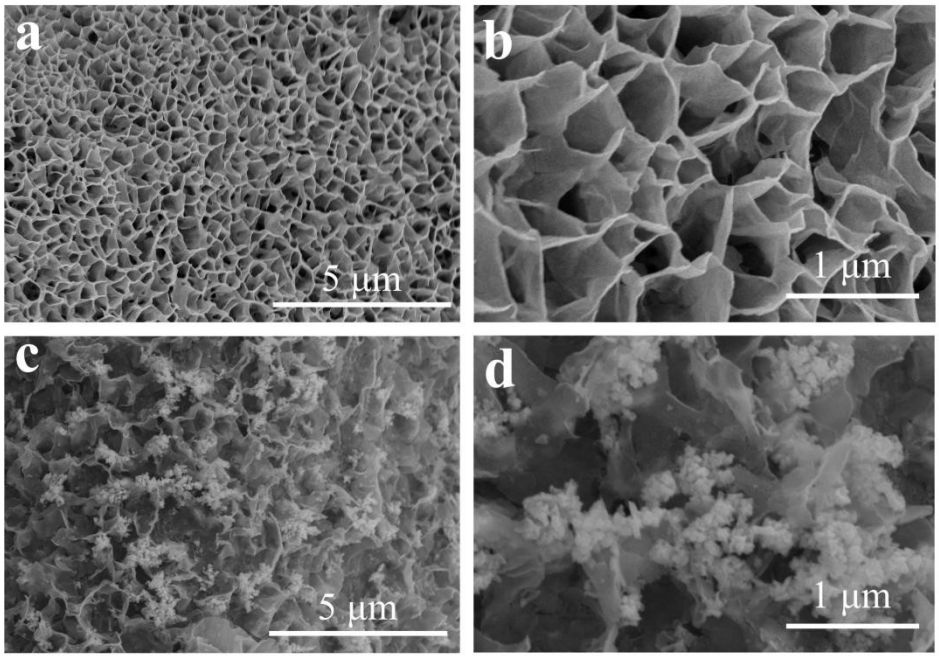

Fig. S17 SEM images of (a-b) NiCo-MOF/NF, (c-d) Pd/NiCo-MOF/NF after HMFOR at 1.40 V *vs.* RHE in 1.0 mol L^{-1} KOH electrolyte with 10.0 mmol L^{-1} HMF.

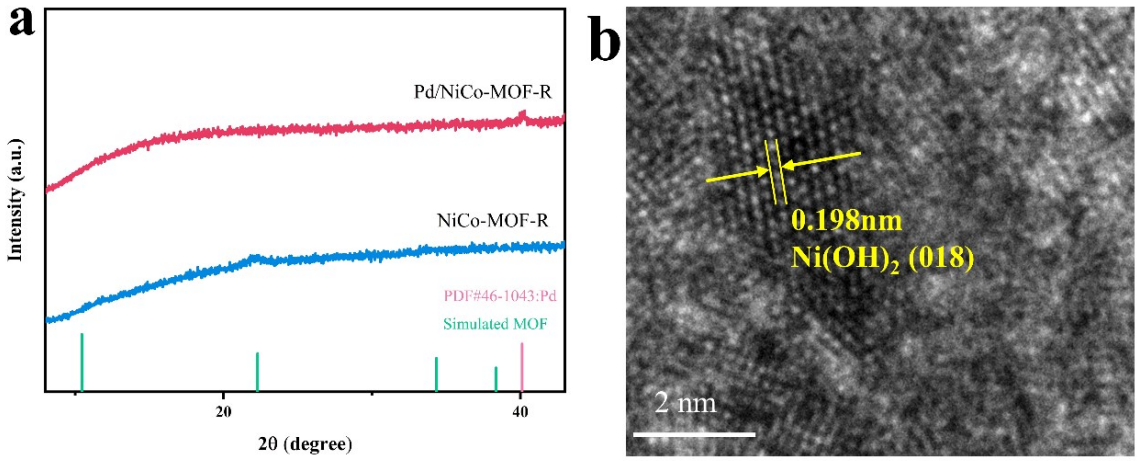

Fig. 18 (a) XRD patterns of catalysts after HMFOR tests, (b) TEM images of Pd/NiCo-MOF/NF after HMFOR.

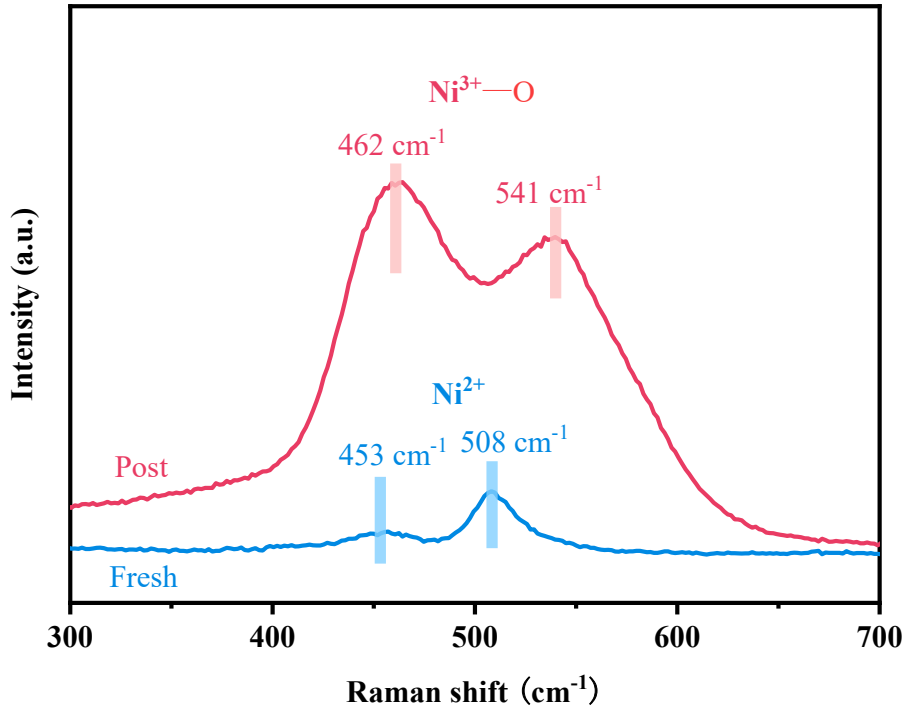

Fig. S19 Raman spectra of Pd/NiCo-MOF/NF before and after HMFOR test.

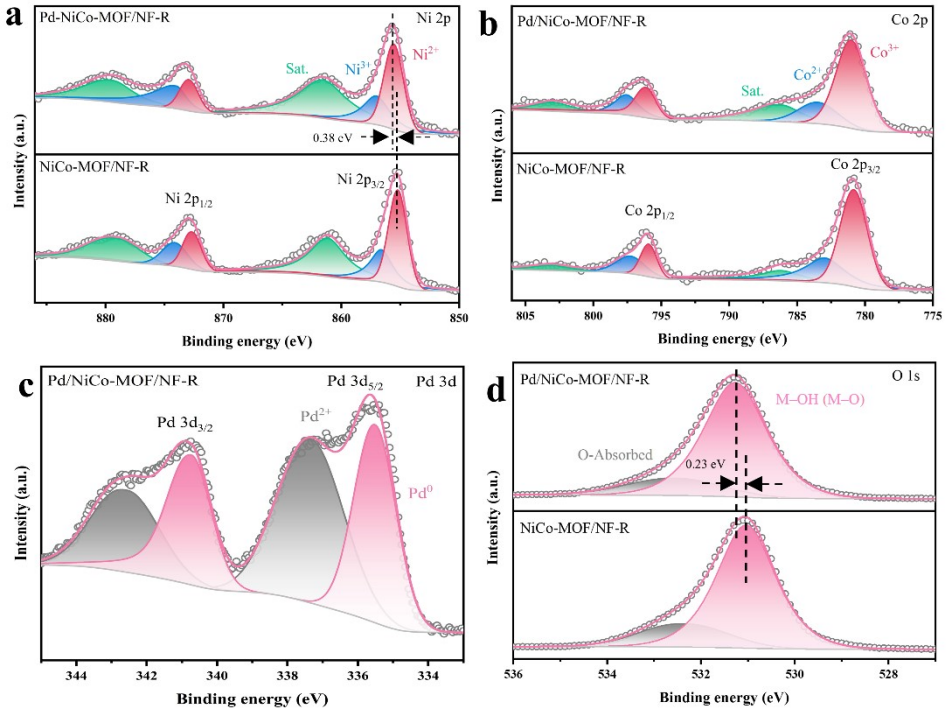

Fig. S20 XPS analysis: (a) Pd 3d, (b-d) O 1s, Ni 2p, and Co 2p spectra of the Pd/NiCo-MOF/NF and NiCo-MOF/NF after HMFOR test.

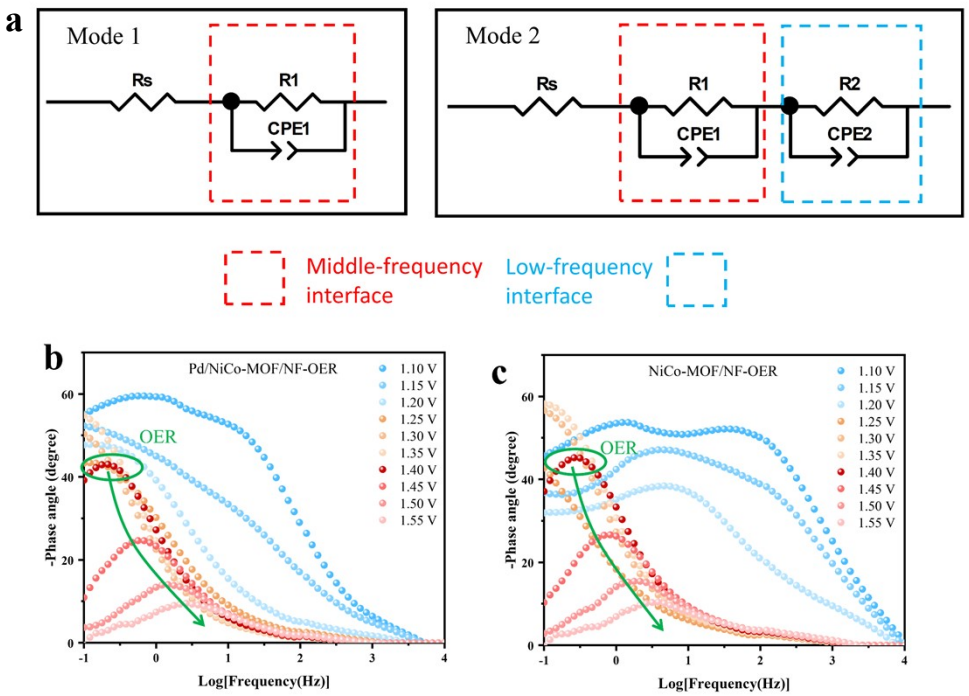

Fig. S21 (a) Two modes for the fitted equivalent circuit. (b-c) Bode plots of the Pd/NiCo-MOF/NF and NiCo-MOF/NF catalysts in 1.0 mol L^{-1} KOH without HMF.

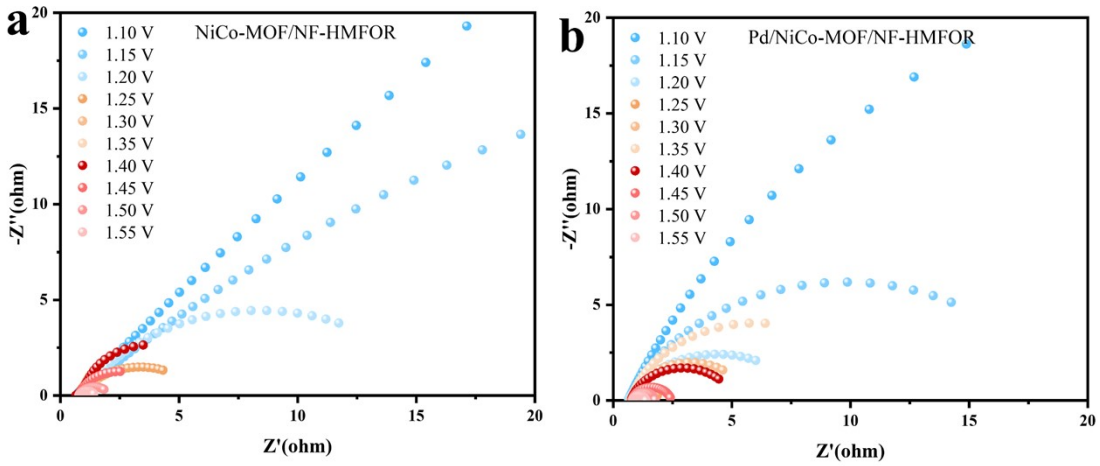

Fig. 22 Nyquist plots of (a) NiCo-MOF/NF and (b) Pd/NiCo-MOF/NF during HMF oxidation (1.0 mol L^{-1} KOH + 30 mmol L^{-1} HMF) under increased potentials.

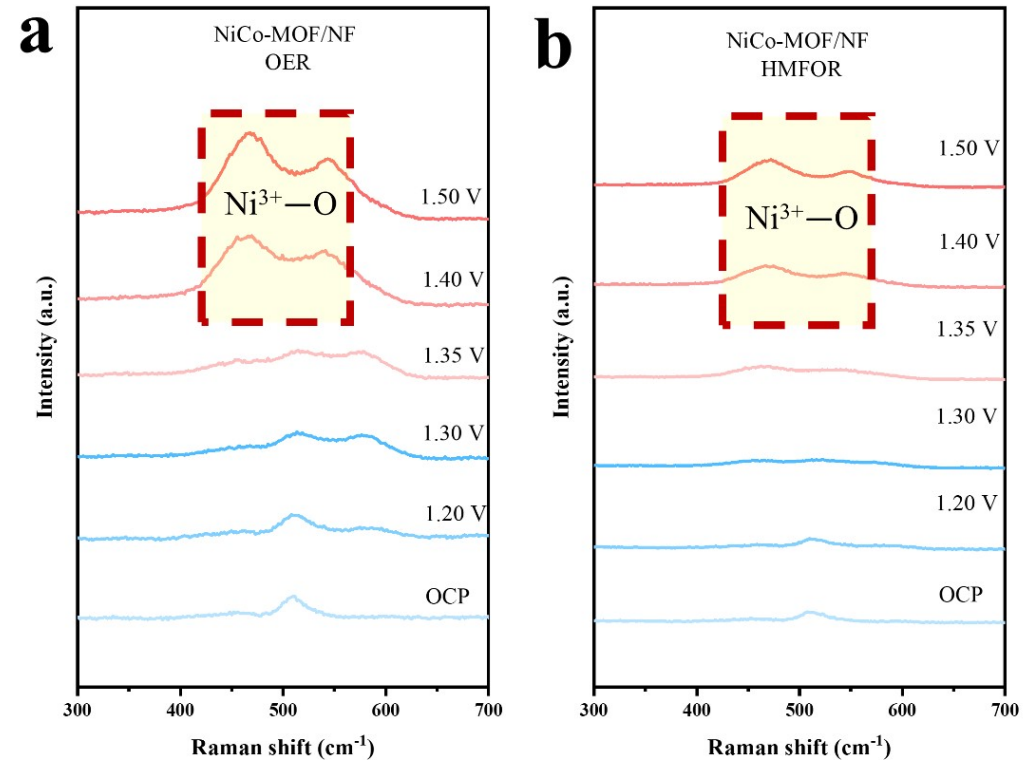

Fig. S23 Quasi-in situ Raman detection of NiCo-MOF/NF during OER and HMFOR.

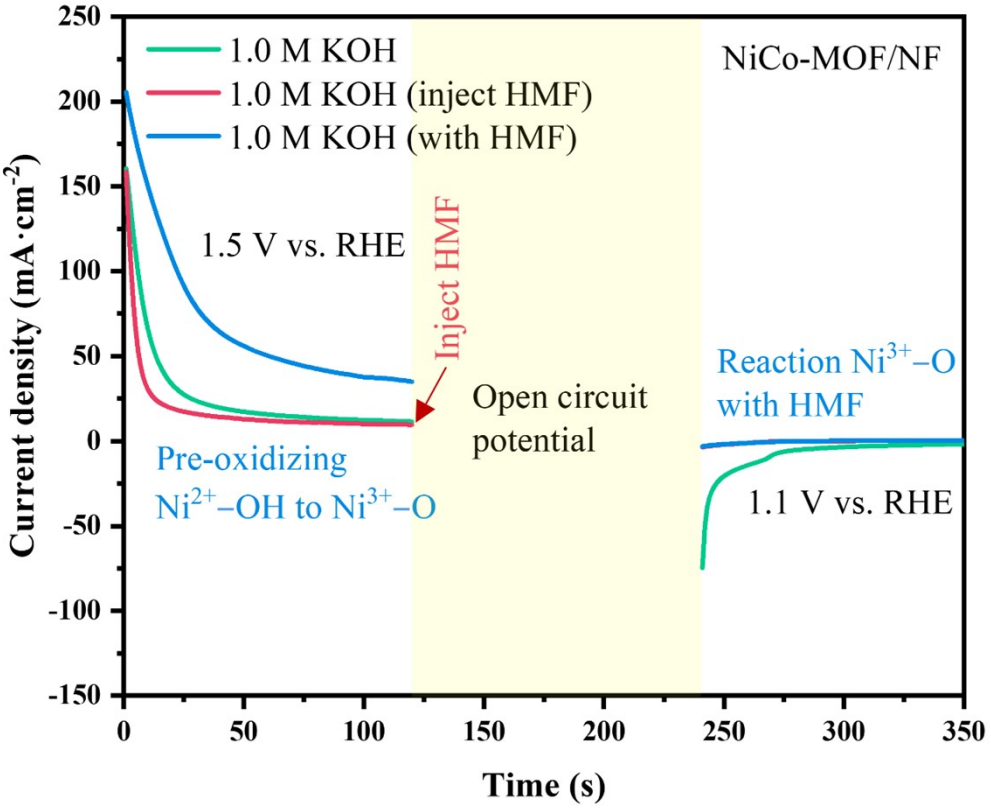

Fig. S24 Muti-potential step curves of NiCo-MOF/NF.

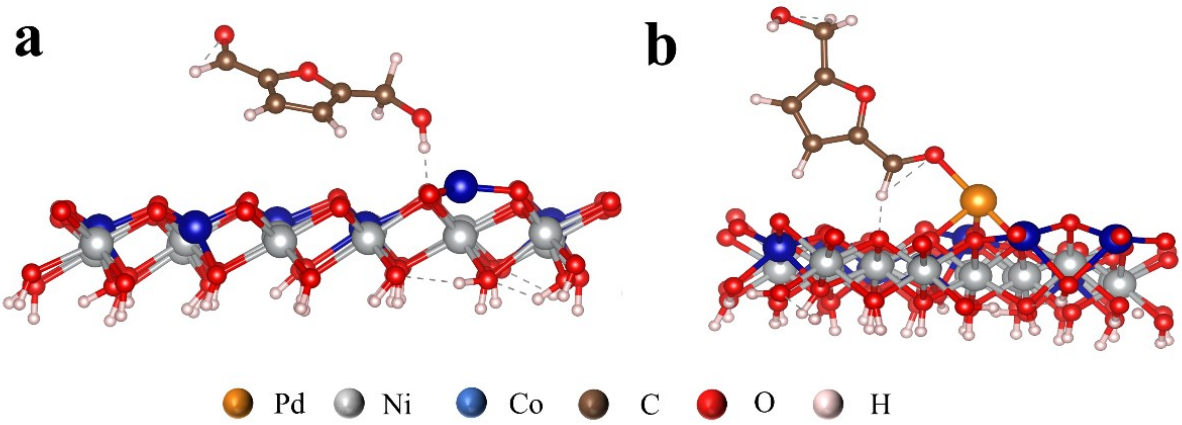

Fig. S25 Comparison of adsorption energies of HMF on (a) NiCo-MOF/NF and (b) PdNiCo-MOF/NF surface.

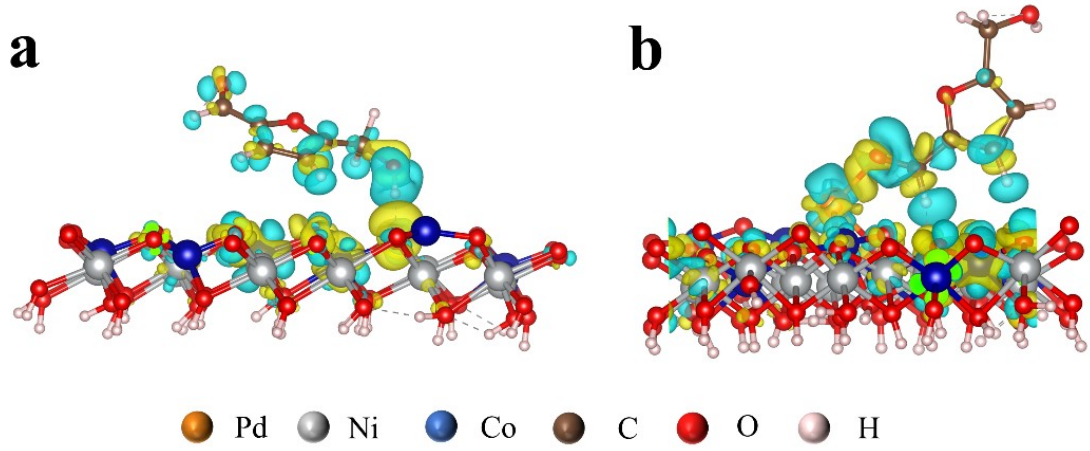

Fig. S26 Charge-density-difference map of the (a) NiCo-MOF/NF and (b) Pd/NiCo-MOF/NF interface; the yellow and cyan isosurfaces denote electron accumulation and depletion, respectively.

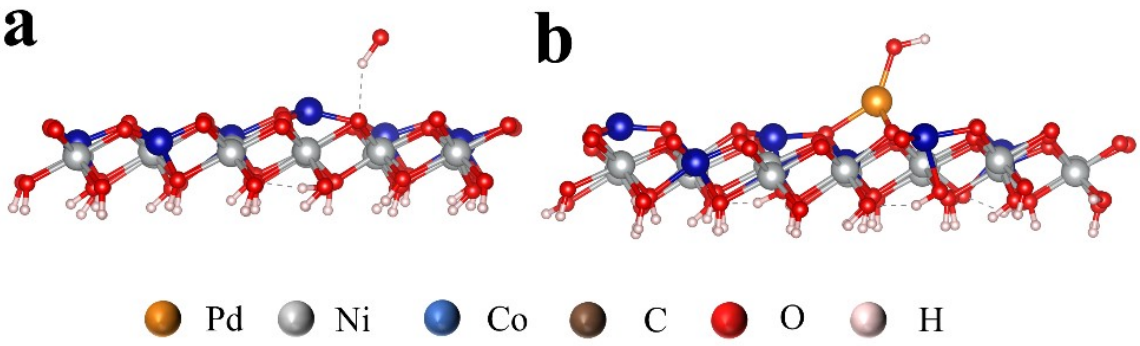

Fig. S27 The adsorption models of OH^* on (a) NiCo-MOF/NF (b) and Pd/NiCo-MOF/NF surface.

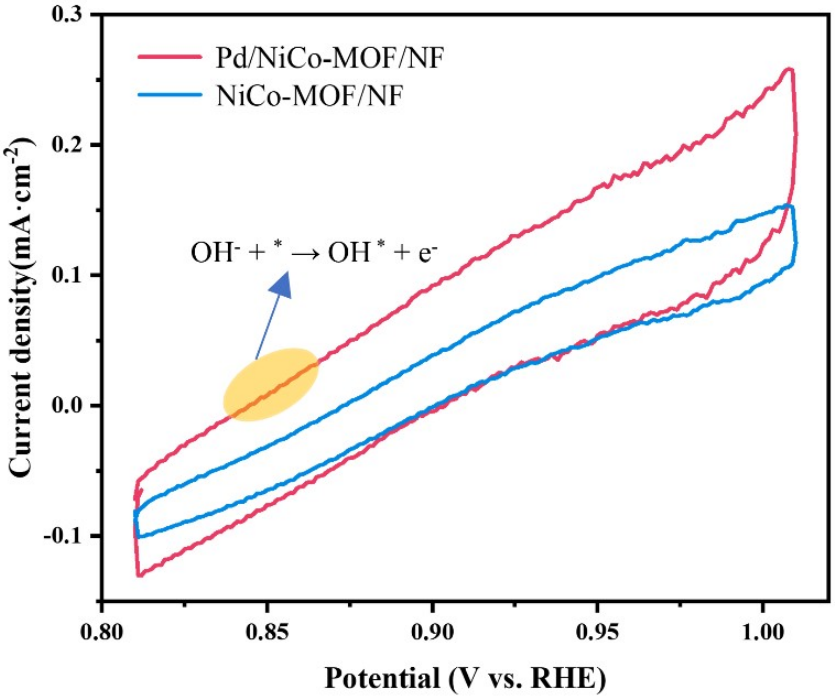

Fig. S28 CV curves of NiCo-MOF/NF and Pd/NiCo-MOF/NF in 1.0 mol L^{-1} KOH and 10.0 mol L^{-1} HMF.

Table S1 The mass loading of NiCo-MOF on Ni foam (1×3 cm^2) determined via gravimetric analysis (partial sample data listed).

Sample	NF (g)	NiCo-MOF/NF (g)	NiCo-MOF Load (mg)
1	0.10975	0.11170	1.95
2	0.11405	0.11606	2.01
3	0.11044	0.11198	1.54
4	0.11386	0.11553	1.67
5	0.11858	0.12004	1.46
6	0.10723	0.10861	1.38
7	0.11442	0.11608	1.66
8	0.09691	0.09841	1.50
9	0.11791	0.11960	1.69

Table S2 Pd loading variation and optimization on Ni Foam determined via gravimetric analysis (1×3 cm^2).

Concentration of Pd deposition solution (mmol L^{-1})	NiCo-MOF/NF(g)	Pd/NiCo-MOF/NF(g)	Pd Load (mg)	Pd(*wt*%)
0.10	0.11198	0.11215	0.17	0.15%
0.15	0.09841	0.09869	0.28	0.28%
0.25	0.11606	0.11643	0.37	0.32%
0.50	0.11960	0.12008	0.48	0.40%

Table S3 ICP-MS analysis of NiCo-MOF/NF and Pd/NiCo-MOF/NF monolithic catalysts.

Sample	Ni (*wt*%)	Co(*wt*%)	Pd(*wt*%)
Pd/NiCo-MOF/NF	96.06	0.55	0.27
NiCo-MOF/NF	95.14	0.67	/

Table S4 TEM-EDS results of Pd/ NiCo-MOF/NF.

Element	Atomic fraction (%)	Mass fraction (%)
Ni	25.8	34.9
Co	11.8	16.0
Pd	12.5	30.7
O	50.0	18.4

Table S5 XPS semi-quantitative content of Pd, Ni, and Co elements in NiCo-MOF/NF and Pd/ NiCo-MOF/NF before and after electrolysis.

Sample	Ni^{3+}[%]	Ni^{2+}[%]	Co^{3+}[%]	Co^{2+}[%]	Pd^{2+}[%]	Pd^{0}[%]
Pd/NiCo-MOF/NF	29.2	70.8	37.4	62.6	19.1	80.9
NiCo-MOF/NF	25.7	74.3	42.0	58.0	/	/
Pd/NiCo-MOF/NF-R	41.9	58.1	21.1	78.9	52.9	47.1
NiCo-MOF/NF-R	37.6	62.4	33.9	66.1	/	/